

Entanglement and quantum transport in integrable systems

Vincenzo Alba¹

¹International School for Advanced Studies (SISSA), Via Bonomea 265, 34136, Trieste, Italy, INFN, Sezione di Trieste
(Dated: March 7, 2024)

Understanding the entanglement structure of out-of-equilibrium many-body systems is a challenging yet revealing task. Here we investigate the entanglement dynamics after a quench from a piecewise homogeneous initial state in integrable systems. This is the prototypical setup for studying quantum transport, and it consists in the sudden junction of two macroscopically different and homogeneous states. By exploiting the recently developed integrable hydrodynamic approach and the quasiparticle picture for the entanglement dynamics, we conjecture a formula for the entanglement production rate after joining two semi-infinite reservoirs, as well as the steady-state entanglement entropy of a finite subregion. We show that both quantities are determined by the quasiparticles created in the Non Equilibrium steady State (NESS) appearing at large times at the interface between the two reservoirs. Specifically, the steady-state entropy coincides with the thermodynamic entropy of the NESS, whereas the entropy production rate reflects its spreading into the bulk of the two reservoirs. Our results are numerically corroborated using time-dependent Density Matrix Renormalization Group (tDMRG) simulations in the paradigmatic XXZ spin-1/2 chain.

I. INTRODUCTION

The quest for a complete understanding of entanglement spreading in out-of-equilibrium many-body system is a fruitful research theme. Recently, this became experimentally relevant, as it is now possible to measure the entanglement dynamics with cold atoms^{1,2}. The best-known entanglement diagnostic tool is the von Neumann (entanglement) entropy $S \equiv -\text{Tr} \rho_A \ln \rho_A$, where ρ_A is the reduced density matrix of a subsystem A (see Figure 1 (a) for a one-dimensional setup).

A prominent out-of-equilibrium situation is that of the quench from two homogeneous initial states. This is a particular instance of *inhomogeneous* quantum quenches. The prototypical setup for spin chains is depicted in Figure 1 (a), and it consists in the sudden junction of two chains A and B that are prepared in two homogeneous *macroscopically* different quantum states $|\Psi_A\rangle$ and $|\Psi_B\rangle$. Subsequently, the state $|\Psi_A\rangle \otimes |\Psi_B\rangle$ is evolved in real time using a quantum many-body Hamiltonian H . Typically, a non-zero current arises between the two chains. The main focus so far has been on transport of local quantities, such as the local energy and local magnetization. Several techniques have been used, such as Conformal Field Theory³⁻⁸ (CFT), free-fermion methods⁹⁻²⁰, field theory methods²¹⁻²³, integrability²⁴⁻²⁸, and numerical techniques^{20,29-33}. For integrable models a recent breakthrough^{34,35} allows for an analytic treatment of transport problems using Thermodynamic Bethe Ansatz (TBA) techniques³⁶⁻⁴⁶.

Surprisingly, as of now there are no exact results for the entanglement dynamics after inhomogeneous quenches. Notable exceptions are systems that can be mapped to CFTs in curved spacetime⁶⁻⁸. In this case it is established that S grows logarithmically after the quench⁷.

In contrast, for *homogeneous* quenches a well-known quasiparticle picture⁴⁷ allows one to understand the entanglement dynamics in terms of quasiparticles traveling ballistically, with opposite quasimomenta, through the system. The underlying idea is that only quasiparticles created at the same point in space are entangled. At a generic time t the entangle-

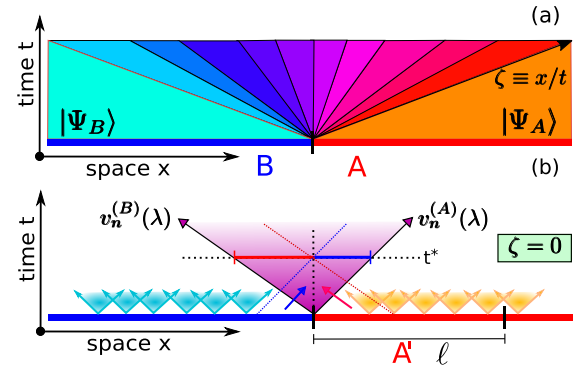


FIG. 1. Entanglement dynamics after the quench from two homogeneous chains in integrable spin chains. (a) At $t = 0$ two chains A and B are prepared in the states $|\Psi_A\rangle$ and $|\Psi_B\rangle$ and are joined. Dynamical properties at fixed $\zeta \equiv x/t$ are described by a thermodynamic Bethe ansatz macrostate. (b) Quasiparticle picture for the entanglement. Shaded cones denote quasiparticle pairs. Different quasiparticles are produced in A and B . The entanglement production rate and its steady-state value are determined by the macrostate with $\zeta = 0$. The larger shaded region is the associated lightcone (note the different velocities $v_n^{(A)}$ and $v_n^{(B)}$). n labels the quasiparticle families. We consider the entanglement between A and B , as well as that of a finite region A' of size ℓ .

ment entropy $S(t)$ between a subregion A and the rest is proportional to the number of quasiparticles emitted at the same point in space at $t = 0$, and being at time t one in subsystem A and the other in B . More quantitatively,

$$S(t) \propto 2t \int_{2|v|t < \ell} d\lambda |v(\lambda)| f(\lambda) + \ell \int_{2|v|t > \ell} d\lambda f(\lambda), \quad (1)$$

where $f(\lambda)$ depends on the cross section for creating quasiparticles with quasimomentum λ , and $v(\lambda)$ is their velocity. Eq. (1) holds in the space-time scaling limit, i.e., $\ell, t \rightarrow \infty$ with fixed t/ℓ . In many physical situations a maximum velocity v_M exists, for instance, due to the Lieb-Robinson bound⁴⁸. Then, Eq. (1) predicts a linear growth for $t \leq \ell/(2v_M)$, fol-

lowed by a volume-law $S \propto \ell$ at longer times. The validity of (1) has been proven rigorously only for free-fermion models^{49–54}, for which $f(\lambda)$ and $v(\lambda)$ can be determined analytically. The quasiparticle picture has been also confirmed in several numerical studies^{55–57}, and using holographic methods^{58–65}. Violations of the quasiparticle picture have been observed in CFT with large central charge^{64,66–70}. Remarkably, a framework to render (1) predictive for generic integrable systems has been developed in Ref. 71 (see Ref. 72 for an application to the Hubbard chain). Specifically, for integrable systems $f(\lambda)$ coincides with the thermodynamic entropy associated with the post-quench steady state, while the quasiparticle velocities $v(\lambda)$ are those of the low-lying excitations around it.

Here by combining a recent hydrodynamic approach for integrable systems^{34,35} with the quasiparticle picture (1), we provide the first exact results for the entanglement dynamics after a global quench from a piecewise homogeneous initial state in generic integrable systems. Specifically, we focus on the steady-state entanglement entropy of a finite region A' (see Figure 1 (b)), as well as the entanglement production rate between two semi-infinite reservoirs. Our main result is that both are determined by the physics of the Non-Equilibrium-Steady-State (NESS) (ray with $\zeta = 0$ in Figure 1 (a)) appearing at the interface between the two reservoirs. The steady-state entanglement entropy coincides with the NESS thermodynamic entropy, whereas the entanglement production rate reflects the spreading of the NESS from the interface into the two reservoirs.

The latter is relevant for quantifying the rate at which quantum information spreads. The study of the quantum information spreading is attracting enormous attention recently. For instance, in the holographic community, the focus has been on the so-called entanglement velocity v_E , which is defined as⁷³ $dS(t)/dt = v_E s_{th} \partial A$, with s_{th} the thermodynamic entropy of the steady state, and ∂A the length of the boundary between the subsystem of interest and the environment. For homogeneous quenches, v_E has been investigated using holographic methods⁷³, exact calculations in free models^{53,74}, and recently in the dynamics obtained from random unitary gates⁷⁵. For inhomogeneous quenches, the information spreading started to be investigated only recently⁷⁶.

II. ENTANGLEMENT VIA INTEGRABLE HYDRODYNAMICS

The first key ingredient to derive our results is that the spectrum of integrable models exhibits families of stable quasiparticles. Typically, these are composite objects of elementary excitations. For spin chains, they correspond to bound states of magnons. The possible set of quasimomenta (rapidities) λ that can be assigned to the quasiparticles are obtained by solving the so-called Bethe equations⁷⁷ (see also Appendix A). In the thermodynamic limit the rapidities form a continuum. Thermodynamic properties of integrable models are described by the particle densities $\rho_n(\lambda)$ and the hole densities $\rho_n^{(h)}(\lambda)$. The latter is the density of unoccupied rapidities. The total

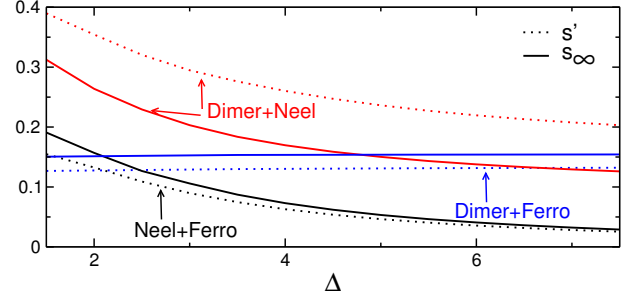


FIG. 2. Entanglement dynamics after the quench from a piecewise homogeneous initial state in the XXZ chain: Theoretical predictions using the integrable hydrodynamics. The steady-state entropy density $s_\infty \equiv \lim_{t \rightarrow \infty} S(t)/\ell$ (full line) and the entanglement production rate $s'(t) \equiv dS(t)/dt$ (dotted line) are plotted versus the chain anisotropy Δ for several initial states.

density is defined as $\rho_n^{(t)} \equiv \rho_n + \rho_n^{(h)}$. Here the subscript n labels different quasiparticle families, and for spin chains is the size of the bound states. For free models in terms of quasimomenta $\rho_n^{(t)} = \text{const}$, reflecting that the quasimomenta are equally-spaced. Every set of $\rho_n, \rho_n^{(h)}$ can be interpreted as a thermodynamic macrostate, which corresponds to an exponentially large number of microscopic eigenstates of the model. Their number is given as $e^{S_{YY}}$, with S_{YY} the so-called Yang-Yang entropy⁷⁸

$$S_{YY} = s_{YY} L = L \sum_{n=1}^{\infty} \int d\lambda [\rho_n^{(t)} \ln \rho_n^{(t)} - \rho_n \ln \rho_n - \rho_n^{(h)} \ln \rho_n^{(h)}] \\ \equiv L \sum_n \int d\lambda s_{YY}^{(n)}[\rho_n, \rho_n^{(h)}]. \quad (2)$$

Similar to free models, S_{YY} counts the number of ways of assigning the different rapidities λ to the quasiparticles, compatibly with the densities $\rho_n, \rho_n^{(h)}$.

The second key ingredient in our approach is the integrable hydrodynamics framework^{34,35}. Due to integrability, information spreads ballistically from the interface between A and B . As a consequence, physical observables depend only on the combination $\zeta \equiv x/t$ (see Figure 1 (a)), with x the distance from the interface between A and B . For each fixed ζ , dynamical properties of local and quasilocal observables are described by a thermodynamic macrostate, i.e., a set of densities $\rho_{\zeta,n}, \rho_{\zeta,n}^{(h)}$. Each macrostate identifies a different Generalized Gibbs Ensemble^{47,79–109}. The macrostate with $\zeta = 0$ is known as Non Equilibrium Steady State (NESS). The central result of Ref. 34 and 35 is that $\rho_{\zeta,n}$ satisfy the continuity equation

$$[\zeta - v_{\zeta,n}(\lambda)] \partial_\zeta \vartheta_{\zeta,n}(\lambda) = 0, \quad (3)$$

where $\vartheta_{\zeta,n} \equiv \rho_{\zeta,n}/\rho_{\zeta,n}^{(t)}$, together with the standard TBA equations⁷⁷

$$\rho_{\zeta,n}^{(t)}(\lambda) = a_n(\lambda) + \sum_{m=1}^{\infty} (a_{n,m} \star \rho_{\zeta,m})(\lambda). \quad (4)$$

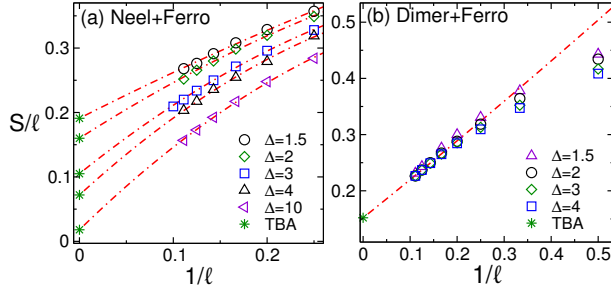


FIG. 3. Steady-state entropy density after the quench from a piecewise initial state in the XXZ chain. Results are for the initial states $|N\rangle \otimes |F\rangle$ and $|MG\rangle \otimes |F\rangle$ (panel (a) and (b), respectively). S/ℓ is plotted against t/ℓ . The symbols are tDMRG data at long times for different Δ . The star symbols are the Bethe ansatz results. Dash-dotted lines are fits to $S/\ell = s_\infty + a/\ell + b/\ell^2$, with a, b fitting parameters, and s_∞ the Bethe ansatz results (Figure 2 (b)).

Here a_n and $a_{n,m}$ are known functions of λ (see Appendix A for their expression for the XXZ chain), and the star symbols denotes the convolution $f \star g \equiv \int d\mu f(\lambda - \mu)g(\mu)$. Crucially, in (3) $v_{\zeta,n}$ are the velocities of the low-lying excitations around the macrostate $\rho_{\zeta,n}$, and fully encode the interactions (scatterings) between quasiparticles¹¹⁰. They can be calculated using standard TBA techniques¹¹⁰ (see Appendix C). The solutions of (3) can be conveniently written as³⁵

$$\vartheta_{\zeta,n}(\lambda) = \theta_H(v_{\zeta,n}(\lambda) - \zeta)(\vartheta_n^B(\lambda) - \vartheta_n^A(\lambda)) + \vartheta_n^A(\lambda), \quad (5)$$

with $\theta_H(x)$ the Heaviside function, and $\vartheta_{\zeta,n}^{A(B)}$ the densities describing the steady states arising after the homogeneous quenches with initial states $|\Psi_A\rangle$ and $|\Psi_B\rangle$, respectively. Exact results for $\vartheta_n^{A(B)}$ are available for several quenches^{111–125} (see also Appendix B). We now present our main results. We start discussing the steady-state entanglement entropy of a finite region A' of length ℓ embedded in part A and placed next to the interface with B (see Figure 1 (b)). The steady-state entropy is obtained in the limit $\ell/t \rightarrow 0$, which identifies the macrostate with $\zeta = 0$ (NESS). Since the spatial extension of the region described by this macrostate increases linearly with time, for $t \gg \ell$ the $\zeta = 0$ macrostate is expected to describe the entire subsystem A' . Similar to Ref. 71, it is natural to conjecture that the entanglement entropy density $s_\infty \equiv \lim_{t \rightarrow \infty} S(t)/\ell$ becomes that of the Yang-Yang entropy of the NESS. The latter is the thermodynamic entropy of the GGE describing (quasi) local observables in space-time regions with $x/t \rightarrow 0$. Using (2), this implies

$$s_\infty = \sum_{n=1}^{\infty} \int d\lambda s_{YY}^{(n)}[\rho_{\zeta=0,n}, \rho_{\zeta=0,n}^{(h)}], \quad (6)$$

where $s_{YY}^{(n)}$ is calculated using the solutions of (3)(4).

We now turn to the entanglement production rate. For homogeneous quenches, this corresponds to the slope of the linear term in (1). Physically, Eq. (1) means that $S(t)$ is determined by the total number of quasiparticles that at time t crossed the interface between A and B . It is natural to assume that the same applies to the inhomogeneous case. After

the quench, the different lightcones associated with different ζ s start spreading from the interface between A and B . For short times, all the types of quasiparticles remain confined within A , the only ones crossing the boundary between A and the rest are the ones described by the $\zeta = 0$ macrostate. At generic time t their number is proportional to the width of the associated lightcone (see Figure 1 (b)). Equivalently, the entanglement growth at short times reflects the spreading of the NESS. Since the lightcone width increases linearly with time, one should expect the linear behavior $S(t) \propto s't$, with $s' \equiv dS(t)/dt$ the entanglement production rate given as

$$s' = \sum_{n=1}^{\infty} \int d\lambda |v_{\zeta=0,n}| s_{YY}^{(n)}[\rho_{\zeta=0,n}, \rho_{\zeta=0,n}^{(h)}]. \quad (7)$$

Formally, Eq. (7) is the same as that for the homogeneous quench conjectured in Ref. 71. However, here the quasiparticle velocities are not odd under parity, i.e., $v_n(\lambda) \neq -v_n(-\lambda)$, implying that the lightcone is not symmetric (in Figure 1(b) $v_n^{(A)}$ and $v_n^{(B)}$ denote the different quasiparticle velocities in the two reservoirs). Similar to the homogeneous case the velocity of the entangling particles depends only on the local equilibrium state at large times⁷¹ (here the NESS). Finally, we should mention that obtaining the full-time dynamics of the entanglement entropy is an arduous task, unlike for homogeneous quenches. The reason is that it requires reconstructing the quasiparticles trajectories. Precisely, since the quasiparticles velocity v is finite, the typical time t^* for the quasiparticles to travel through the subsystem is $t^* \sim \ell$, with ℓ the subsystem size. This implies that these quasiparticles should be described by $\zeta = \ell/t^* = \mathcal{O}(1)$. A possible direction to determine the quasiparticle trajectories is to use the approach of Ref. 126.

In the following we provide numerical evidence for (6) and (7) considering the anisotropic spin-1/2 Heisenberg chain (XXZ chain). The Hamiltonian reads

$$H_{XXZ} = J \sum_{i=1}^L [S_i^x S_{i+1}^x + S_i^y S_{i+1}^y + \Delta S_i^z S_{i+1}^z]. \quad (8)$$

Here $S_i^{x,y,z} \equiv \sigma_i^{x,y,z}/2$ are spin-1/2 operators, L the chain length and Δ the anisotropy parameter. We set $J = 1$ in (8), restricting ourselves to $\Delta > 1$. The XXZ chain is the paradigm of Bethe ansatz solvable models⁷⁷ (see Appendix A).

We consider the inhomogeneous quenches in which parts A or B are prepared in the Néel state $|N\rangle \equiv (|\uparrow\downarrow\uparrow\downarrow\cdots\rangle + |\downarrow\uparrow\downarrow\uparrow\cdots\rangle)/\sqrt{2}$, the Majumdar-Ghosh or dimer state $|MG\rangle \equiv (|\uparrow\uparrow\rangle + |\downarrow\downarrow\rangle)/\sqrt{2}$, and the ferromagnetic state $|F\rangle \equiv |\uparrow\uparrow\cdots\rangle$. For all these cases the bulk densities $\vartheta_n^{A(B)}$ (cf. (5)) are known analytically (see Appendix B). Also, for $\Delta > 1$ the dynamics from states obtained by joining states with opposite magnetization¹⁰⁹ leads to diffusive or subdiffusive transport^{127–129}. In contrast, all the initial states considered here lead to ballistic transport (see Appendix D).

The strategy to use (6) and (7) is to first solve the coupled systems of integral equations (3) and (4) for $\zeta = 0$. The obtained densities $\rho_{\zeta=0,n}, \rho_{\zeta=0,n}^{(h)}$ (some numerical results are

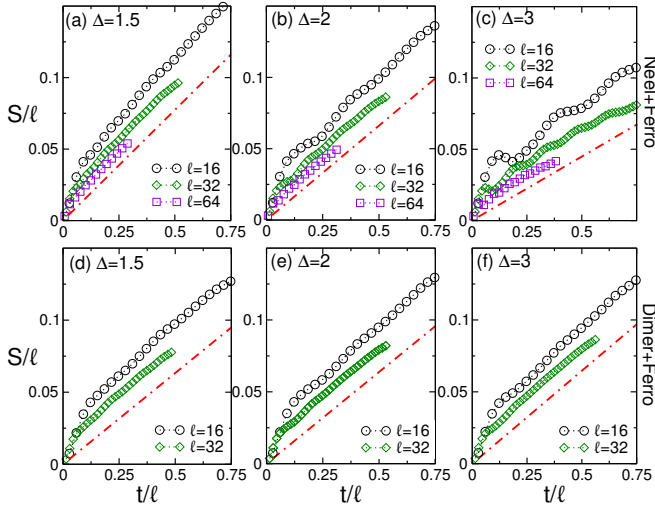


FIG. 4. Entanglement dynamics after the quench from a piecewise homogeneous initial state in the XXZ chain: Entanglement production rate. Panels (a,b,c) and (d,e,f) show tDMRG results for the initial states $|N\rangle \otimes |F\rangle$ and $|MG\rangle \otimes |F\rangle$, respectively. Different symbols are for different Δ and $\ell \leq 64$. S/ℓ is plotted versus the rescaled time t/ℓ . The dash-dotted line is the theoretical result using Bethe ansatz (Figure 2) in the thermodynamic limit $\ell \rightarrow \infty$.

shown in Appendix E) are then substituted in (2) (6) and (7). Our results are summarized in Figure 2. The Figure shows the steady-state entropy s_∞ (dotted lines) and the entanglement production rate s' as a function of Δ . For the quench with initial state $|N\rangle \otimes |F\rangle$, both s_∞ and s' vanish for $\Delta \rightarrow \infty$, reflecting that the Néel state is the ground state of the XXZ chain in that limit. Interestingly, for both $|N\rangle \otimes |F\rangle$ and $|MG\rangle \otimes |F\rangle$, since the ferromagnet is an exact eigenstate of the XXZ chain at any Δ , no quasiparticle production happens in subsystem A . As a consequence, $S(t)$ is fully determined by the quasiparticle transport from B to A . However, s_∞ and $s'(t)$ are smaller than the corresponding values for the homogeneous quench from the Néel state and the dimer state⁷¹. It is also interesting to observe that for these quenches only the quasiparticles with $n = 1$ contribute in (6) and (7), i.e., the bound states contribution to the entanglement vanishes (see Appendix E). This is not the case for the quench from $|MG\rangle \otimes |F\rangle$, for which all bound states contribute and quasiparticles are generated in both reservoirs. In this case both s_∞ and s' exhibit a rather weak dependence on Δ (see Figure 2).

III. NUMERICAL CHECKS IN THE XXZ CHAIN

We now turn to verify the theoretical predictions presented in Figure 2 using tDMRG simulations^{130–134}. We first focus on the steady-state entropy density s_∞ of a finite block A' of length ℓ (Figure 1 (b)). We consider only the quenches from the states $|N\rangle \otimes |F\rangle$ and $|MG\rangle \otimes |F\rangle$, as they are easier to simulate. In fact, in our tDMRG simulations we use the comparatively small value of the bond dimension $\chi \approx 75$. This allows us to obtain reliable results, provided that a space-time

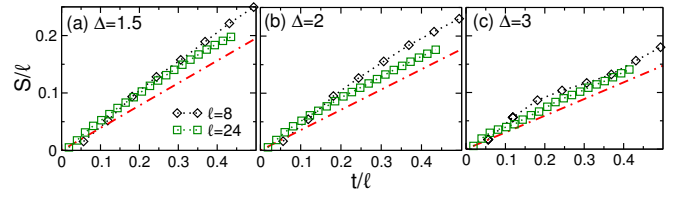


FIG. 5. The same as in Figure 4 for the initial state $|N\rangle \otimes |MG\rangle$. Notice the smaller subsystems sizes ($\ell \leq 24$) as compared with Figure 4. The different panels are for different Δ . The dash-dotted lines are the Bethe ansatz results.

average of the data is performed. This surprising efficiency of tDMRG for transport-related quantities has been also observed in Ref. 135.

Our tDMRG results in the regime $t \gg \ell$ are reported in Figure 3 (a) and (b), plotting s_∞ versus $1/\ell$. The raw tDMRG data at any time after the quench are reported in Appendix F. To minimize the effects of oscillating (with the block size) scaling corrections we averaged the data for $t \gg \ell$. The results are for chains with $L = 40$ sites, several Δ s (different symbols), and $\ell \leq 10$. The star symbols are the Bethe ansatz results (6). The dash-dotted lines are fits to $S/\ell = s_\infty + a/\ell + b/\ell^2$, with s_∞ the thermodynamic limit results, and a, b fitting parameters. Finite-size corrections are clearly visible for small ℓ . However, for both initial states the numerical data are compatible in the thermodynamic limit with the Bethe ansatz results. Note that for the quench from $|MG\rangle \otimes |F\rangle$ the dependence on Δ for large ℓ is not visible within the numerical precision, as expected from Figure 2.

We now focus on the entanglement production rate in Figure 4, again considering the quench from $|N\rangle \otimes |F\rangle$ (panels (a)-(c)) and $|MG\rangle \otimes |F\rangle$ (panels (d)-(e)), plotting S/ℓ versus t/ℓ . The data are now for chains with $L \leq 128$. We always consider the half-chain entropy, i.e., $A' = A$ and A half of the chain (see Figure 1). A crucial consequence is that only one boundary is present between A' and the rest. The dash-dotted lines are the Bethe ansatz predictions (Figure 2 and (7)). After an initial transient, in all cases $S(t)$ exhibits linear behavior. The slope of this linear increase is in agreement with the Bethe ansatz results, already for $\ell \approx 16$. A more systematic analysis of finite-size corrections is presented in Appendix G. For the quench from $|MG\rangle \otimes |F\rangle$, again, one should observe the weak dependence on Δ . Finally, in Figure 5 we show the results for the initial state $|N\rangle \otimes |MG\rangle$. Due to the large amount of entanglement, we can only provide reliable tDMRG data for $\ell \leq 24$. tDMRG simulations are performed with $\chi = 400$. To highlight finite-size and finite-time corrections we show data for $\ell = 8$, which exhibit large deviations from the Bethe ansatz predictions. On the other hand, for $\ell = 24$ the data are clearly compatible with (7).

IV. CONCLUSIONS

We investigated the entanglement dynamics after the quench from a piecewise initial state in integrable mod-

els. We conjectured an analytic formula for the entanglement production rate after joining two semi-infinite reservoirs as well as for the steady-state entropy of a finite subregion ((6) and (7), respectively). Our work opens several promising new directions. For instance, it would be interesting to consider the inhomogeneous quench in which an integrability-breaking term acting at the interface between A and B is added to the Hamiltonian. Already in the case of a defect that preserves integrability this gives non trivial effects³⁵. It would be also enlightening to consider a time-dependent bipartition in which subsystem A' moves away from the boundary. By appropriately tuning the speed at which A' changes its position, it should be possible to change the thermodynamic macrostate governing the entanglement production. It should be possible to extend the method to treat the mutual information, as done for free fermions^{136,137}. Finally, it would be interesting to extend the quasiparticle picture to treat multipartite systems as in Ref.¹³⁸.

ACKNOWLEDGMENTS

I am very grateful to Bruno Bertini for clarifying discussions on several aspects of the integrable hydrodynamic approach. I also acknowledge very fruitful discussions with Maurizio Fagotti and Pasquale Calabrese. This work was supported by the European Union's Horizon 2020 research and innovation programme under the Marie Skłodowska-Curie grant agreement No 702612 OEMBS.

Appendix A: Bethe ansatz solution of the XXZ chain

Due to the conservation of the total magnetization S_z , the eigenstates of the XXZ can be classified according to the total magnetization $S_T = \sum_i S_i^z$. Equivalently, one can use the total number M of down spins as a good quantum number for the eigenstates.

In the Bethe ansatz⁷⁷ solution of the XXZ chain, the eigenstates in the sector with M down spins (particles) are identified by a set of M rapidities λ_j , which are solutions of the so-called Bethe equations⁷⁷

$$\left[\frac{\sin(\lambda_j + i\frac{\eta}{2})}{\sin(\lambda_j - i\frac{\eta}{2})} \right]^L = - \prod_{k=1}^M \frac{\sin(\lambda_j - \lambda_k + i\eta)}{\sin(\lambda_j - \lambda_k - i\eta)}, \quad (\text{A1})$$

where $\eta \equiv \text{arccosh}(\Delta)$. Here we are interested in the thermodynamic limit $L, M \rightarrow \infty$ with M/L fixed. Then, the solutions of the Bethe equations (A1) form string patterns in the complex plane. Rapidities forming a n -string can be written as

$$\lambda_{n,\gamma}^j = \lambda_{n,\gamma} + i\frac{\eta}{2}(n+1-2j) + \delta_{n,\gamma}^j, \quad (\text{A2})$$

where $j = 1, \dots, n$ denotes the different string components, $\lambda_{n,\gamma}$ is the “string center”, and $\delta_{n,\gamma}^j$ are the string deviations. For the majority of the eigenstates of the XXZ chain, the string deviations are exponentially small, i.e., $\delta_{n,\gamma}^j = \mathcal{O}(e^{-L})$

(string hypothesis). The n -strings describe bound states of n down spins. The string centers $\lambda_{n,\gamma}$ are obtained by solving the Bethe-Gaudin-Takahashi (BGT) equations⁷⁷

$$L\theta_n(\lambda_{n,\alpha}) = 2\pi I_{n,\alpha} + \sum_{(n,\alpha) \neq (m,\beta)} \Theta_{n,m}(\lambda_{n,\alpha} - \lambda_{m,\beta}). \quad (\text{A3})$$

For $\Delta > 1$, one has $\lambda_{n,\gamma} \in [-\pi/2, \pi/2]$. Here we used that $\theta_n(\lambda) \equiv 2 \arctan[\tan(\lambda)/\tanh(n\eta/2)]$. The scattering phases $\Theta_{n,m}(\lambda)$ are given as

$$\Theta_{n,m}(\lambda) \equiv (1 - \delta_{n,m})\theta_{|n-m|}(\lambda) + 2\theta_{|n-m|+2}(\lambda) + \dots + \theta_{n+m-2}(\lambda) + \theta_{n+m}(\lambda). \quad (\text{A4})$$

Each choice of the so-called BGT quantum numbers $I_{n,\alpha} \in \frac{1}{2}\mathbb{Z}$ corresponds to a different set of solutions of (A3), i.e., to a different eigenstate of the chain. The corresponding eigenstate energy E and total momentum P are obtained by summing over all the rapidities as $E = \sum_{n,\alpha} \epsilon_n(\lambda_{n,\alpha})$, and $P = \sum_{n,\alpha} z_n(\lambda_{n,\alpha})$ with

$$\epsilon_n(\lambda) \equiv -\frac{\sinh(\eta) \sinh(n\eta)}{\cosh(n\eta) - \cos(2\lambda)}, \quad z_n(\lambda_{n,\alpha}) = \frac{2\pi I_{n,\alpha}}{L}. \quad (\text{A5})$$

In the thermodynamic limit, one works with the rapidity densities. The root densities $\rho_{n,p}$ are formally defined as

$$\rho_{n,p}(\lambda) \equiv \lim_{L \rightarrow \infty} \frac{1}{L(\lambda_{n,\alpha+1} - \lambda_{n,\alpha})}. \quad (\text{A6})$$

It is also convenient to define the associated hole densities $\rho_{n,h}$, i.e., the density of unoccupied rapidities, and the total densities $\rho_{n,t} = \rho_n + \rho_{n,h}$. The BGT equations (A3) in the thermodynamic limit become a system of integral equations

$$\rho_n^{(t)}(\lambda) = a_n(\lambda) + \sum_{n=1}^{\infty} (a_{n,m} \star \rho_m)(\lambda), \quad (\text{A7})$$

where we defined

$$a_{nm}(\lambda) = (1 - \delta_{nm})a_{|n-m|}(\lambda) + 2a_{|n-m|}(\lambda) + \dots + 2a_{n+m-2}(\lambda) + a_{n+m}(\lambda), \quad (\text{A8})$$

with

$$a_n(\lambda) = \frac{1}{\pi} \frac{\sinh(n\eta)}{\cosh(n\eta) - \cos(2\lambda)}. \quad (\text{A9})$$

Appendix B: Macrostates for homogeneous quenches

Here we report the analytical results for the root densities $\vartheta_n^{(A)}(\lambda)$ and $\vartheta_n^{(B)}(\lambda)$ (see the main text). We consider the homogeneous quenches from the Néel state and the Majumdar-Ghosh state. These densities characterize the thermodynamic macrostate in the bulk of the two systems A and B , i.e., for $|\zeta| \rightarrow \infty$. We first define the densities $\eta_n \equiv \rho_{n,h}/\rho_n$. In terms of η_n one has $\theta_n = 1/(1 + \eta_n)$.

For both the Néel state and the Majumdar-Ghosh state, the η_n obey the recursive equation^{97,121}

$$\eta_n(\lambda) = \frac{\eta_{n-1}(\lambda + i\frac{\eta}{2})\eta_{n-1}(\lambda - i\frac{\eta}{2})}{1 + \eta_{n-2}(\lambda)} - 1, \quad (\text{B1})$$

$$\rho_{n,h}(\lambda) = \rho_{n,t}(\lambda + i\frac{\eta}{2}) + \rho_{n,t}(\lambda) - \rho_{n-1,h}(\lambda), \quad (\text{B2})$$

where $\eta_0 = 0$ and $\rho_{0,h} = 0$.

For the Néel state one has¹²¹

$$\eta_1 = \frac{2[2 \cosh(\eta) + 2 \cosh(3\eta) - 3 \cos(2\lambda) \sin^2(\lambda)]}{[\cosh(\eta) - \cos(2\lambda)][\cosh(4\eta) - \cos(4\lambda)]} \quad (\text{B3})$$

$$\rho_{1,h} = a_1 \left(1 - \frac{\cosh^2(\eta)}{a_1 \pi^2 \sin^2(2\lambda) + \cosh^2(\eta)} \right),$$

For the Majumdar-Ghosh one has^{113,120}

$$\eta_1 = \frac{\cos(4\lambda) - \cosh(2\eta)}{\cos^2 \lambda (\cos(2\lambda) - \cosh(2\eta))} - 1, \quad (\text{B4})$$

and

$$\rho_{1,h} = a_1(\lambda) + \frac{1}{2\pi} (\omega(\lambda - i\eta/2) + \omega(\lambda + i\eta/2)), \quad (\text{B5})$$

with

$$\omega(\lambda) = -\frac{\sinh(\eta)(-2 + \cosh(\eta) + 2 \cosh(2\eta))}{4(\cos(2\lambda) - \cosh(2\eta))^2} + \frac{3 \cosh(3\eta) + 4 \cos(2\lambda)(-\cosh(\eta) + \sinh^2(\eta))}{4(\cos(2\lambda) - \cosh(2\eta))^2}. \quad (\text{B6})$$

Appendix C: Velocities of entangling quasiparticles

A crucial ingredient in the integrable hydrodynamic approach^{34,35} and in the derivation of our results is the velocity of the low-lying excitations around the TBA macrostates $\rho_n, \rho_n^{(h)}$. Here we outline its derivation following the approach of Ref. 110. Given a generic thermodynamic macrostate identified by some densities $\rho_n, \rho_n^{(h)}$, one can imagine choosing among the eigenstates of the XXZ chain a representative of the macrostate. This would be identified by some BGT quantum numbers $I_{n,\alpha}^*$. Low-lying excitations around it can be constructed as particle-hole excitations. In each n -string sector, these correspond to the change $I_{n,h}^* \rightarrow I_{n,p}$, where $I_{n,p}(I_{n,h}^*)$ is the BGT number of the added particle (hole). Since the model is interacting, this local change in quantum numbers affects *all* the rapidities obtained by solving the new set of Bethe equations. The excess energy of the particle-hole excitation can be written as¹¹⁰

$$\delta E_n = e_n(\lambda_{n,p}^*) - e_n(\lambda_{n,h}^*). \quad (\text{C1})$$

Note that (C1) is the same as for free models apart from the dressing of the single particle energy. The change in the total momentum is obtained from (A5) as

$$\delta P = z_n(\lambda_{n,p}^*) - z_n(\lambda_{n,h}^*). \quad (\text{C2})$$

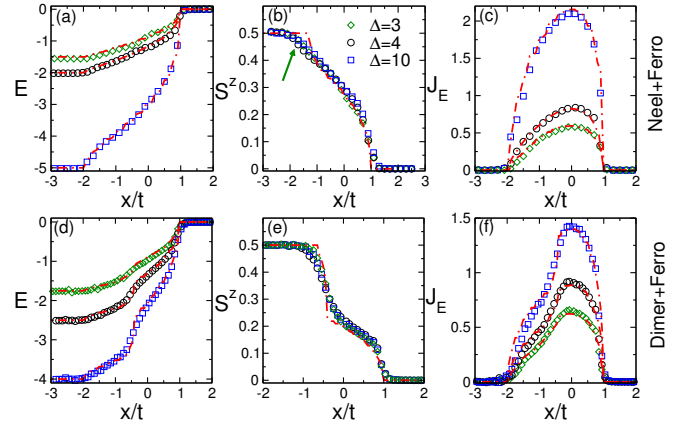


FIG. 6. Quantum transport in the XXZ chain after the quench from piecewise homogeneous initial state. Panels (a,b,c) show results for the initial state $|N\rangle \otimes |F\rangle$. Panels (d,e,f) are for the initial state $|MG\rangle \otimes |F\rangle$. The figure reports the local energy density E , the local magnetization S^z , and the energy current J_E plotted versus $\zeta = x/t$, with x the position in the chain, measured from the interface between the two reservoirs. In all panels the symbols are tDMRG data for a chain with $L = 300$ and several values of Δ . To obtain smooth behavior a space-time average was performed in a window with $\zeta = x/t \pm \epsilon$ and $\epsilon \approx 0.1$. The dash dotted lines are the theoretical predictions using the Bethe ansatz.

The group velocity associated with the particle-hole excitations is by definition

$$v_n^*(\lambda) \equiv \frac{\partial e_n}{\partial z_n} = \frac{e'_n(\lambda)}{2\pi\rho_n(1 + \eta_n(\lambda))}, \quad (\text{C3})$$

where we used that⁷⁷ $dz_n(\lambda)/d\lambda = 2\pi\rho_{n,t}$, and we defined $e'_n(\lambda) = de_n(\lambda)/d\lambda$. Here $e'_n(\lambda)$ is obtained by solving an infinite system of Fredholm integral equations of the second kind¹¹⁰

$$e'_n(\lambda) + \frac{1}{2\pi} \sum_{m=1}^{\infty} \int d\mu e'_m(\mu) \frac{\Theta'_{m,n}(\mu - \lambda)}{1 + \eta_m^*(\mu)} = e'_n(\lambda), \quad (\text{C4})$$

where $\Theta'_{n,m}(\lambda) \equiv d\Theta_{n,m}(\lambda)/d\lambda$ and $e'_n(\lambda) \equiv de_n(\lambda)/d\lambda$ (cf. also (A4) and (A5)).

Appendix D: Integrable hydrodynamics: Conserved charges and currents

In this section we provide some numerical checks of the integrable hydrodynamics approach^{34,35}, focusing on the XXZ chain in the region with $\Delta > 1$. We consider the quenches with initial states $|N\rangle \otimes |F\rangle$ and $|MG\rangle \otimes |F\rangle$. Using tDMRG simulations we investigate the dynamics of the local magnetization S^z , the local energy density E , and the energy current

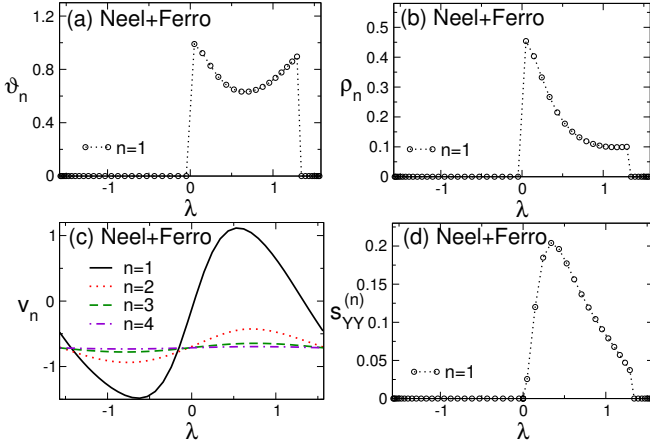


FIG. 7. Integrable hydrodynamics approach for the quench from the state $|N\rangle \otimes |F\rangle$. The results are for the XXZ chain with $\Delta = 2$. Panel (a) plots the densities ϑ_n as a function of the rapidity λ for $\zeta = 0$. For $n > 1$ one has $\vartheta_n = 0$. Note that ϑ_1 is nonzero only for $\lambda > 0$. Panel (b): Density ρ_n as a function of λ . Similar to (a) only ρ_1 is nonzero for $\lambda > 0$, whereas $\rho_n = 0$ for $n > 1$. Panel (c): group velocities of the quasiparticles excitations v_n plotted as a function of λ . Different lines correspond to different families of excitations (bound states). Note that for $n > 1$, one has that $v_n < 0$ at any λ , whereas v_1 changes sign at $\lambda = 0$. Note also that v_n have no well defined parity, in contrast with homogeneous quenches for which $v_n(\lambda) = -v_n(-\lambda)$. (d) Contributions to the Yang-Yang entropy of the different quasiparticles families plotted versus λ . Only $n = 1$ gives nonzero contribution for $\lambda > 0$.

J_E . These are defined as³⁵

$$S^z \equiv S_i^z \quad (D1)$$

$$E \equiv S_i^x S_{i+1}^x + S_i^y S_{i+1}^y + \Delta S_i^z S_{i+1}^z - \frac{\Delta}{4}, \quad (D2)$$

$$J_E \equiv S_{i-1}^x S_i^z S_{i+1}^y - S_{i-1}^y S_i^z S_{i+1}^x - \Delta S_{i-1}^z S_i^x S_{i+1}^y + \Delta S_{i-1}^z S_i^y S_{i+1}^x - \Delta S_{i-1}^x S_i^y S_{i+1}^z + \Delta S_{i-1}^y S_i^x S_{i+1}^z. \quad (D3)$$

In the framework of the Bethe ansatz, these are written in terms of the root densities $\rho_{\zeta,n}(\lambda)$ as

$$S_z = \sum_n n \int d\lambda \rho_{\zeta,n}, \quad (D4)$$

$$E = \sum_n \int d\lambda \rho_{\zeta,n} \frac{\sinh \eta \sinh(n\eta)}{\cos(2\lambda) - \cosh(n\eta)}, \quad (D5)$$

$$J_E = \sum_n \int d\lambda \rho_{\zeta,n} \frac{\sin(2\lambda) \sinh^2 \eta \sinh(r\eta)}{(\cos(2\lambda) - \cosh(n\eta))^2}. \quad (D6)$$

Note that all the observables are functions of $\zeta \equiv x/t$. The dependence on ζ is encoded in the densities $\rho_{\zeta,n}$ ³⁵.

The Bethe ansatz results (D4)(D5)(D6) are compared with tDMRG results in Figure 6. The upper and lower panels show tDMRG data for the quench with initial states $|N\rangle \otimes |F\rangle$ and $|MG\rangle \otimes |F\rangle$, respectively. The data are for the XXZ chain with $L = 300$ sites, up to times $t \lesssim 100$. The results in

panels (a-c) are obtained using bond dimension $\chi \sim 20$. For the quench from the state $|MG\rangle \otimes |F\rangle$ (panels (e-f)) we used $\chi \sim 75$. In all panels the different symbols correspond to different values of Δ . In order to remove spatial and temporal oscillations, we performed a spatio-temporal average. Specifically, for each fixed ζ the results in the Figure are obtained by averaging the data in a window $\zeta \pm \epsilon$ with $\epsilon \approx 0.1$. The dash-dotted lines are the theoretical results (D4)(D5)(D6). For $|\zeta| \gg 1$ all the observables become ζ independent. This happens in spatio-temporal regions with $|x| \gg v_M t$, with v_M the maximum velocity in the system. Remarkably, for both quenches, and for all values of Δ , the tDMRG data are in very good agreement with the Bethe ansatz. Note, however, that the theoretical predictions exhibits some cusp-like behaviors (see for instance the arrow in panel (b)). These are expected and have been discussed in Ref. 139, although they are not well reproduced by the tDMRG results. It is natural to expect that these deviations should be attributed to the finite χ and to the finite-time and finite-size effects.

Appendix E: Neel-Ferro quench: Bethe ansatz results

In this section we provide some details on the Bethe ansatz results for the quench from the state $|N\rangle \otimes |F\rangle$. Our results are summarized in Figure 9.

Specifically, panels (a) and (b) show the densities $\vartheta_{\zeta,n}$ and $\rho_{\zeta,n}$, respectively. The results are for $\zeta = 0$, which identifies the relevant macrostate to describe the entanglement dynamics after the quench (the subscript ζ in $\vartheta_{\zeta,n}$ and $\rho_{\zeta,n}$ is omitted in the Figure). First, it is interesting to observe that only $\vartheta_{\zeta,1}$ and $\rho_{\zeta,1}$ are nonzero. Moreover, ϑ_1 is nonzero only for $\lambda > 0$. Similar behavior is observed for ρ_1 (see panel (b)).

The group velocities of the low-lying excitations around the macrostate with $\zeta = 0$ are reported in Figure 9 (c). These are obtained by numerically solving (C4) and using (C3). As anticipated in the main text, one has $v_n(\lambda) \neq -v_n(-\lambda)$. This is in stark contrast with homogeneous quenches, where one has⁷¹ $v_n(\lambda) = -v_n(-\lambda)$. As a consequence the lightcone of the entangling quasiparticles is not symmetric. It is also interesting to observe that for any λ , $v_n < 0$ for $n > 1$, which implies that there is no transport of bound states from B to A after the quench.

Finally, in Figure 9 (e) we show the contributions to the Yang-Yang entropy density $s_{YY}^{(n)}$ (see its definition in the main text) of the quasiparticles. Clearly, only quasiparticles with $n = 1$ and $\lambda > 0$ contribute to the entropy. Together with the results in panel (c), this implies that the entanglement between the two subsystems is generated by the transport of particles from B to A .

Appendix F: Steady-state entropy: DMRG data

In this section we discuss in more detail the numerical data for the steady-state entanglement entropy presented in Figure 3 in the manuscript, i.e., for the quench from the state $|N\rangle \otimes |F\rangle$. We consider the entanglement entropy of a subsystem A'

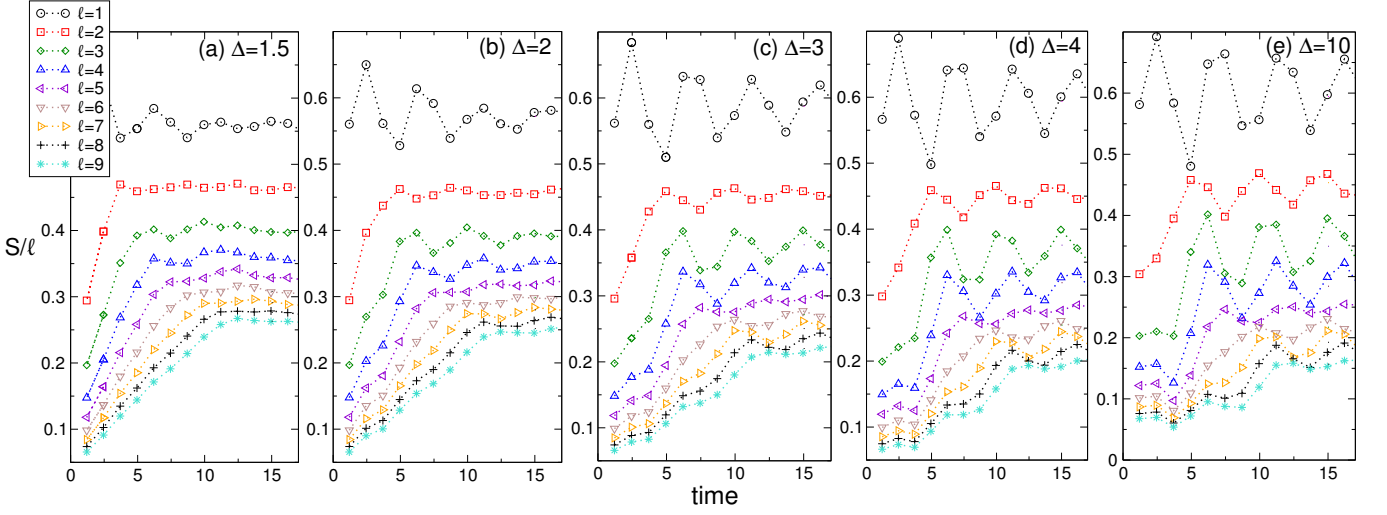


FIG. 8. Entanglement dynamics after the quench from a piecewise homogeneous initial state in the XXZ chain: Results for initial $|N\rangle \otimes |F\rangle$. The figure shows S/ℓ plotted versus time. The different panels are for different values of Δ . The symbols are tDMRG data for several values of the subsystem length ℓ and for a chain with $L = 40$ sites.

of length ℓ placed next to the boundary between A and B . To avoid boundary effects A' is embedded in A , which is chosen larger than A' .

Our tDMRG results are presented in Figure 8. The data are obtained using standard tDMRG simulations with bond dimension $\chi \sim 300$ for the XXZ chain with $L = 40$ sites and $t \sim 16$. To calculate the von Neumann entropy we employed the techniques described in Ref. 140. The different panels correspond to different values of $1.5 \leq \Delta \leq 10$. The figure shows S/ℓ plotted versus the time after the quench. In each panel the different symbols are for subsystems of different length $1 \leq \ell \leq 9$. For each ℓ a linear increase, followed by a saturation, is observed. The saturation value decreases upon increasing Δ , in agreement with the theoretical predictions. For $t \rightarrow \infty$, in the limit $\ell \rightarrow \infty$, the entropy density S/ℓ should converge to the Bethe ansatz predictions. However, strong finite-size effects are visible in the Figure, due to the small ℓ considered. Moreover, it is interesting to observe that upon increasing Δ , the data exhibit strong oscillations with time. The data presented in Figure 3 correspond to the time average of the tDMRG data in the time window $13 \leq t \leq 16$. Finally, we should mention that similar results are obtained for the quench from the state $|MG\rangle \otimes |F\rangle$.

Appendix G: Scaling corrections

In this section we discuss in more detail the finite-size corrections of the tDMRG data in Figure 4 in the manuscript. We focus on the quench from the state $|N\rangle \otimes |F\rangle$, for which the largest system subsystem sizes up to $\ell = 64$ are available. We consider the scaling corrections to the entanglement production rate. Figure 9 shows the deviations $\delta S/\ell$ plotted versus the rescaled time t/ℓ . The theory predictions are obtained using formula (7). The different curves in Figure 9

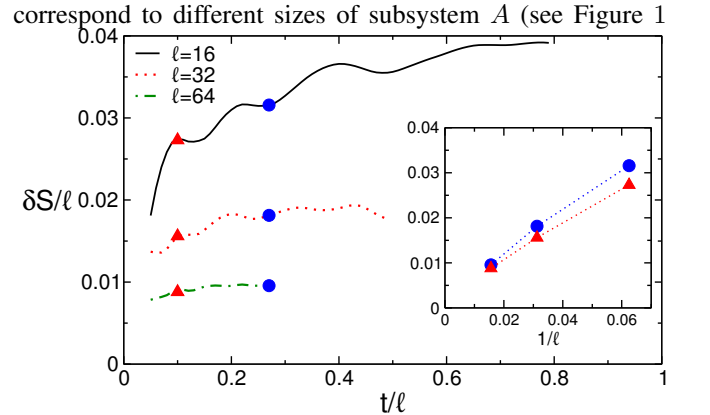


FIG. 9. Entanglement production rate for the quench from the $|N\rangle \otimes |F\rangle$ quench: finite-size corrections. In the main panel the curves are the deviations $\delta S/\ell$ from the Bethe ansatz predictions for the quench with $\Delta = 1.75$ (panel (a) in Figure 4 in the manuscript). Here $\delta S/\ell$ is plotted against the rescaled time t/ℓ . The different curves correspond to the different subsystem sizes $\ell = 16, 32, 64$. Corrections are clearly vanishing in the scaling limit. Inset: $1/\ell$ behavior of the scaling corrections. Here $\delta S/\ell$ at fixed $t/\ell \approx 0.1$ and $t/\ell \approx 0.27$ (data are marked with the same symbols in the main panel) is plotted versus $1/\ell$.

in the manuscript). Clearly, corrections are vanishing in the scaling limit $t, \ell \rightarrow \infty$ with fixed ratio t/ℓ . Interestingly, the dependence of the corrections on t/ℓ becomes weaker upon increasing ℓ . By comparing the data for $\ell = 32$ and $\ell = 64$, it is clear that corrections decay as $1/\ell$ in the thermodynamic limit. This is supported in the inset of Figure 9 showing the data for fixed $t/\ell \approx 0.1$ and $t/\ell \approx 0.27$ plotted versus $1/\ell$. We should mention that a similar behavior as $1/\ell$ has been observed for homogeneous quenches⁷¹.

- ¹ R. Islam, R. Ma, P. M. Preiss, M. E. Tai, A. Lukin, M. Rispoli, and M. Greiner, Measuring entanglement entropy in a quantum many-body system, *Nature* **528**, 77 (2015).
- ² A. M. Kaufman, M. E. Tai, A. Lukin, M. Rispoli, R. Schittko, P. M. Preiss, and M. Greiner, Quantum thermalization through entanglement in an isolated many-body system, *Science* **353**, 794 (2016).
- ³ S. Sotiriadis and J. Cardy, Inhomogeneous Quantum Quenches, *J. Stat. Mech.* (2008) P11003.
- ⁴ D. Bernard and B. Doyon, Energy flow in non-equilibrium conformal field theory, *J. Phys. A: Math. Theor.* **45** (2012), 362001.
- ⁵ M. J. Bhaseen, B. Doyon, A. Lucas, and K. Schalm, Far from equilibrium energy flow in quantum critical systems, *Nat. Phys.* **11**, 509 (2015).
- ⁶ N. Allegra, J. Dubail, J.-M. Stephan, and J. Viti, Inhomogeneous field theory inside the arctic circle, *J. Stat. Mech.* (2016) 053108.
- ⁷ J. Dubail, J.-M. Stephan, J. Viti, and P. Calabrese, Conformal Field Theory for Inhomogeneous One-dimensional Quantum Systems: the Example of Non-Interacting Fermi Gases, *SciPost Phys.* **2**, 002 (2017).
- ⁸ J. Dubail, J.-M. Stephan, and P. Calabrese, Emergence of curved light-cones in a class of inhomogeneous Luttinger liquids, *arXiv:1705.00679*.
- ⁹ V. Eisler, F. Igloi, and I. Peschel, Entanglement in spin chains with gradients, *J. Stat. Mech.* (2009) P02011.
- ¹⁰ A. De Luca, J. Viti, D. Bernard, and B. Doyon, Non-equilibrium thermal transport in the quantum Ising chain, *Phys. Rev. B* **88**, 134301 (2013).
- ¹¹ T. Sabetta and G. Misguich, Non-equilibrium steady states in the quantum XXZ spin chain, *Phys. Rev. B* **88**, 245114 (2013).
- ¹² V. Eisler and Z. Racz, Full counting statistics in a propagating quantum front and random matrix spectra, *Phys. Rev. Lett.* **110**, 060602 (2013).
- ¹³ V. Alba and F. Heidrich-Meisner, Entanglement spreading after a geometric quench in quantum spin chains, *Phys. Rev. B* **90**, 075144 (2014).
- ¹⁴ M. Collura and G. Martelloni, Non-equilibrium transport in d-dimensional non-interacting Fermi gases, *J. Stat. Mech.* (2014) P08006.
- ¹⁵ A. De Luca, G. Martelloni, and J. Viti, Stationary states in a free fermionic chain from the quench action method, *Phys. Rev. A* **91**, 021603(R). (2015).
- ¹⁶ V. Eisler, F. Maislinger, H. G. Evertz, Universal front propagation in the quantum Ising chain with domain-wall initial states *SciPost Phys.* **1**, 014 (2016).
- ¹⁷ J. Viti, J.-M. Stephan, J. Dubail, and M. Haque, Inhomogeneous quenches in a fermionic chain: exact results, *EPL* **115** (2016) 40011.
- ¹⁸ M. Kormos, Inhomogeneous quenches in the transverse field Ising chain: scaling and front dynamics, *arXiv:1704.03744*.
- ¹⁹ G. Peretto and A. Gambassi, Ballistic front dynamics after joining two semi-infinite quantum Ising chains, *arXiv:1704.03437*.
- ²⁰ L. Vidmar, D. Iyer, and M. Rigol, Emergent Eigenstate Solution to Quantum Dynamics Far from Equilibrium, *Phys. Rev. X* **7**, 021012 (2017).
- ²¹ A. De Luca, J. Viti, L. Mazza, and D. Rossini, Energy transport in Heisenberg chains beyond the Luttinger liquid paradigm, *Phys. Rev. B* **90**, 161101 (2014).
- ²² O. Castro-Alvaredo, Y. Chen, B. Doyon, and M. Hoogeveen, Thermodynamic Bethe ansatz for non-equilibrium steady states: exact energy current and fluctuations in integrable QFT, *J. Stat. Mech.* (2014) P03011.
- ²³ A. Biella, A. De Luca, J. Viti, D. Rossini, L. Mazza, and R. Fazio, Energy transport between two integrable spin chains, *Phys. Rev. B* **93**, 205121 (2016).
- ²⁴ X. Zotos, F. Naef, and P. Prelovsek, Transport and conservation laws, *Phys. Rev. B* **55**, 11029 (1997).
- ²⁵ X. Zotos, Finite Temperature Drude Weight of the One-Dimensional Spin-1/2 Heisenberg Model, *Phys. Rev. Lett.* **82**, 1764 (1999).
- ²⁶ T. Prosen, Open XXZ Spin Chain: Nonequilibrium Steady State and a Strict Bound on Ballistic Transport, *Phys. Rev. Lett.* **106**, 217206 (2011).
- ²⁷ T. Prosen and E. Ilievski, Families of Quasilocal Conservation Laws and Quantum Spin Transport, *Phys. Rev. Lett.* **111**, 057203 (2013).
- ²⁸ E. Ilievski, M. Medenjak, and T. Prosen, Quasilocal Conserved Operators in the Isotropic Heisenberg Spin-1/2 Chain, *Phys. Rev. Lett.* **115**, 120601 (2015).
- ²⁹ F. Heidrich-Meisner, A. Honecker, D. C. Cabra, and W. Brenig, Zero-frequency transport properties of one-dimensional spin- $\frac{1}{2}$ systems, *Phys. Rev. B* **68**, 134436.
- ³⁰ D. Gobert, C. Kollath, U. Schollwöck, and G. Schütz, Real-time dynamics in spin-1/2 chains with adaptive time-dependent density matrix renormalization group, *Phys. Rev. E* **71**, 036102 (2005).
- ³¹ S. Langer, F. Heidrich-Meisner, J. Gemmer, I. P. McCulloch, and U. Schollwöck, Real-time study of diffusive and ballistic transport in spin-1/2 chains using the adaptive time-dependent density matrix renormalization group method, *Phys. Rev. B* **79**, 214409 (2009).
- ³² C. Karrasch, J. H. Bardarson, and J. E. Moore, Finite-Temperature Dynamical Density Matrix Renormalization Group and the Drude Weight of Spin-1/2 Chains, *Phys. Rev. Lett.* **108**, 227206 (2012).
- ³³ C. Karrasch, R. Ilan, and J. E. Moore, Nonequilibrium thermal transport and its relation to linear response, *Phys. Rev. B* **88**, 195129 (2013).
- ³⁴ O. A. Castro-Alvaredo, B. Doyon, and T. Yoshimura, Emergent hydrodynamics in integrable systems out of equilibrium, *Phys. Rev. X* **6**, 041065 (2016).
- ³⁵ B. Bertini and M. Fagotti, Determination of the Nonequilibrium Steady State Emerging from a Defect, *Phys. Rev. Lett.* **117**, 130402 (2016).
- ³⁶ B. Doyon and T. Yoshimura, A note on generalized hydrodynamics: inhomogeneous fields and other concepts, *arXiv:1611.08225*.
- ³⁷ B. Doyon and T. Yoshimura, A note on integrable hydrodynamics: inhomogeneous fields and other concepts, *arXiv:1611.08225*.
- ³⁸ A. De Luca, M. Collura, and J. De Nardis, Non-equilibrium spin transport in the XXZ chain: steady spin currents and emergence of magnetic domains, *arXiv:1612.07265*.
- ³⁹ B. Doyon and H. Spohn, Dynamics of hard rods with initial domain wall state, *arXiv:1703.05971*.
- ⁴⁰ B. Doyon, J. Dubail, R. Konik, and T. Yoshimura, Generalized hydrodynamics and density waves in interacting one-dimensional Bose gases, *arXiv:1704.04151*.
- ⁴¹ B. Doyon, H. Spohn, and T. Yoshimura, A geometric viewpoint on generalized hydrodynamics, *arXiv:1704.04409*.
- ⁴² B. Doyon, T. Yoshimura, and J.-S. Caux, Soliton gases and generalized hydrodynamics, *arXiv:1704.05482*.
- ⁴³ V. B. Bulchandani, R. Vasseur, C. Karrasch, J. E. Moore, Bethe-Boltzmann Hydrodynamics and Spin Transport in the XXZ

- Chain arXiv:1702.06146.
- ⁴⁴ V. B. Bulchandani, R. Vasseur, C. Karrasch, J. E. Moore, Solvable Hydrodynamics of Quantum Integrable Systems, arXiv:1704.03466.
 - ⁴⁵ E. Ilievski and J. De Nardis, On the Microscopic Origin of Ideal Conductivity, arXiv:1702.02930.
 - ⁴⁶ B. Doyon and H. Spohn, Drude Weight for the Lieb-Liniger Bose Gas, arXiv:1705.08141.
 - ⁴⁷ P. Calabrese and J. Cardy, Evolution of Entanglement Entropy in One-Dimensional Systems, J. Stat. Mech. (2005) P04010.
 - ⁴⁸ E. H. Lieb and D. W. Robinson, The finite group velocity of quantum spin systems, Commun. Math. Phys. **28**, 251 (1972).
 - ⁴⁹ M. Fagotti and P. Calabrese, Evolution of entanglement entropy following a quantum quench: Analytic results for the XY chain in a transverse magnetic field, Phys. Rev. A **78**, 010306 (2008).
 - ⁵⁰ V. Eisler and I. Peschel, Entanglement in a periodic quench, Ann. Phys. (Berlin) **17**, 410 (2008).
 - ⁵¹ M. Ghasemi Nezhadhighi, and M. A. Rajabpour, Entanglement dynamics in short and long-range harmonic oscillators, Phys. Rev. B **90**, 205438 (2014).
 - ⁵² A. Coser, E. Tonni, and P. Calabrese, Entanglement negativity after a global quantum quench, J. Stat. Mech. P12017 (2014).
 - ⁵³ J. S. Cotler, M. P. Hertzberg, M. Mezei, and M. T. Mueller, Entanglement Growth after a Global Quench in Free Scalar Field Theory, JHEP **11** (2016) 166.
 - ⁵⁴ A. S. Buyskikh, M. Fagotti, J. Schachenmayer, F. H. L. Essler, and A. J. Daley, Entanglement growth and correlation spreading with variable-range interactions in spin and fermionic tunneling models, Phys. Rev. A **93**, 053620 (2016).
 - ⁵⁵ G. De Chiara, S. Montangero, P. Calabrese, and R. Fazio, Entanglement Entropy dynamics in Heisenberg chains, J. Stat. Mech. P03001 (2006).
 - ⁵⁶ A. M. Läuchli and C. Kollath, Spreading of correlations and entanglement after a quench in the one-dimensional Bose-Hubbard model, J. Stat. Mech. P05018 (2008).
 - ⁵⁷ H. Kim and D. A. Huse, Ballistic Spreading of Entanglement in a Diffusive Nonintegrable System, Phys. Rev. Lett. **111**, 127205 (2013).
 - ⁵⁸ V. E. Hubeny, M. Rangamani, and T. Takayanagi, A Covariant holographic entanglement entropy proposal, JHEP **0707**, 062 (2007);
 - ⁵⁹ J. Abajo-Arrestia, J. Aparicio, and E. Lopez, Holographic Evolution of Entanglement Entropy, JHEP **1011** 149 (2010).
 - ⁶⁰ T. Albash and C. V. Johnson, Evolution of Holographic Entanglement Entropy after Thermal and Electromagnetic Quenches, New J. Phys. **13**, 045017 (2011).
 - ⁶¹ A. Allais and E. Tonni, Holographic evolution of the mutual information, JHEP **1201** 102 (2012).
 - ⁶² R. Callan, J.-Y. He, and M. Headrick, Strong subadditivity and the covariant holographic entanglement entropy formula, JHEP **1206**, 081 (2012).
 - ⁶³ H. Liu and S. J. Suh, Entanglement Tsunami: Universal Scaling in Holographic Thermalization, Phys. Rev. Lett. **112**, 011601 (2014).
 - ⁶⁴ V. Balasubramanian, A. Bernamonti, N. Copland, B. Craps, and F. Galli, Thermalization of mutual and tripartite information in strongly coupled two dimensional conformal field theories, Phys. Rev. D **84**, 105017 (2011).
 - ⁶⁵ H. Liu and S. J. Suh, Entanglement growth during thermalization in holographic systems, Phys. Rev. D **89**, 066012 (2014).
 - ⁶⁶ C. T. Asplund and A. Bernamonti, Mutual information after a local quench in conformal field theory, Phys. Rev. D **89**, 066015 (2014).
 - ⁶⁷ C. T. Asplund, A. Bernamonti, F. Galli, and T. Hartmann, Entanglement Scrambling in 2d Conformal Field Theory, JHEP **09**, 110 (2015).
 - ⁶⁸ S. Leichenauer and M. Moosa, Entanglement Tsunami in (1+1)-Dimensions, Phys. Rev. D **92**, 126004 (2015).
 - ⁶⁹ S. Kundu and J. F. Pedraza, Spread of entanglement for small subsystems in holographic CFTs, Phys. Rev. D **95**, 086008 (2017).
 - ⁷⁰ S. F. Lokhande, G. W. J. Oling, and J. F. Pedraza, Linear response of entanglement entropy from holography, arXiv:1705.10324.
 - ⁷¹ V. Alba and P. Calabrese, Entanglement and thermodynamics after a quantum quench in integrable systems, arXiv:1608.00614.
 - ⁷² M. Mestyán, B. Bertini, L. Piroli, and P. Calabrese, Exact solution for the quench dynamics of a nested integrable system, arXiv:1705.00851.
 - ⁷³ H. Liu and S. J. Suh, Phys. Rev. Lett. **112**, 011601 (2014). H. Liu and S. J. Suh, Phys. Rev. D **89**, 066012 (2014). T. Hartman and J. Maldacena, JHEP **5**, 014 (2013). M. Alishahiha, A. Faraji Astaneh, and M. R. Mohammadi Mozaffar, Phys. Rev. D **90**, 046004 (2014). P. Fonda, L. Franti, V. Keränen, E. Keski-Vakkuri, L. Thorlacius, and E. Tonni, JHEP **8**, 51 (2014). T. Hartman and N. Afkhami-Jeddi, arXiv:1512.02695. M. Mezei, arXiv:1612.00082. D. Roberts and B. Swingle, Phys. Rev. Lett. **117**, 091602 (2016).
 - ⁷⁴ H. Casini, H. Liu, and M. Mezei, JHEP **7**, 77 (2016). M. Mezei and D. Stanford, JHEP **5**, 065 (2017).
 - ⁷⁵ C. von Keyserlingk, T. Rakovsky, F. Pollmann, and S. Sondhi, arXiv:1705.09810. A. Nahum, J. Ruhman, S. Vijay, and J. Haah, Phys. Rev. X **7**, 031016 (2017). A. Nahum, S. Vijay, and J. Haah, arXiv:1705.08975.
 - ⁷⁶ J. Erdmenger, D. Fernandez, M. Flory, E. Megias, A.-K. Straub, and P. Witkowski, Time evolution of entanglement for holographic steady state formation, arXiv:1705.04696.
 - ⁷⁷ M. Takahashi, *Thermodynamics of one-dimensional solvable models*, Cambridge University Press, Cambridge, 1999.
 - ⁷⁸ C. N. Yang and C.P. Yang, Thermodynamics of a One-Dimensional System of Bosons with Repulsive Delta Function Interaction, J. Math. Phys. **10**, 1115 (1969).
 - ⁷⁹ Rigol M, Dunjko V, and Olshanii M. Thermalization and its mechanism for generic isolated quantum systems. Nature **452**, 854 (2008).
 - ⁸⁰ A. Polkovnikov, K. Sengupta, A. Silva, and M. Vengalattore, *Colloquium: Nonequilibrium dynamics of closed interacting quantum systems*, Rev. Mod. Phys. **83**, 863 (2011).
 - ⁸¹ M. Rigol, V. Dunjko, V. Yurovsky, and M. Olshanii, Relaxation in a Completely Integrable Many-Body Quantum System: An *Ab Initio* Study of the Dynamics of the Highly Excited States of 1D Lattice Hard-Core Bosons, Phys. Rev. Lett. **98**, 050405 (2007).
 - ⁸² M. A. Cazalilla, Effect of Suddenly Turning on Interactions in the Luttinger Model, Phys. Rev. Lett. **97**, 156403 (2006).
 - ⁸³ T. Barthel and U. Schollwöck, Dephasing and the Steady State in Quantum Many-Particle Systems, Phys. Rev. Lett. **100**, 100601 (2008).
 - ⁸⁴ M. Cramer, C. W. Dawson, J. Eisert, and T. J. Osborne, Exact Relaxation in a Class of Nonequilibrium Quantum Lattice Systems, Phys. Rev. Lett. **100**, 030602 (2008).
 - ⁸⁵ M. Cramer and J. Eisert, A quantum central limit theorem for non-equilibrium systems: exact local relaxation of correlated states, New J. Phys. **12**, 055020 (2010).
 - ⁸⁶ P. Calabrese, F. H. L. Essler, and M. Fagotti, Quantum Quench in the Transverse-Field Ising Chain, Phys. Rev. Lett. **106**, 227203 (2011).
 - ⁸⁷ M. A. Cazalilla, A. Iucci, and M.-C. Chung, Thermalization and quantum correlations in exactly solvable models, Phys. Rev. E

- 85**, 011133 (2012).
- ⁸⁸ P. Calabrese, F. H. L. Essler, and M. Fagotti, Quantum Quench in the Transverse Field Ising Chain II: Stationary State Properties, *J. Stat. Mech.* (2012) P07022.
 - ⁸⁹ S. Sotiriadis, D. Fioretto, and G. Mussardo, Zamolodchikov-Faddeev Algebra and Quantum Quenches in Integrable Field Theories, *J. Stat. Mech.* (2012) P02017.
 - ⁹⁰ M. Collura, S. Sotiriadis, and P. Calabrese, Equilibration of a Tonks-Girardeau Gas Following a Trap Release, *Phys. Rev. Lett.* **110**, 245301 (2013).
 - ⁹¹ M. Collura, S. Sotiriadis, and P. Calabrese, Quench dynamics of a Tonks-Girardeau gas released from a harmonic trap, *J. Stat. Mech.* P09025 (2013).
 - ⁹² M. Fagotti and F. H. L. Essler, Stationary behaviour of observables after a quantum quench in the spin-1/2 Heisenberg XXZ chain, *J. Stat. Mech.* (2013) P07012.
 - ⁹³ M. Fagotti, M. Collura, F. H. L. Essler, and P. Calabrese, Relaxation after quantum quenches in the spin-1/2 Heisenberg XXZ chain, *Phys. Rev. B* **89**, 125101 (2014).
 - ⁹⁴ M. Kormos, M. Collura, and P. Calabrese, Analytic results for a quantum quench from free to hard-core one-dimensional bosons, *Phys. Rev. A* **89**, 013609 (2014).
 - ⁹⁵ G. Delfino, Quantum quenches with integrable pre-quench dynamics, *J. Phys. A* **47** (2014) 402001.
 - ⁹⁶ S. Sotiriadis and P. Calabrese, Validity of the GGE for quantum quenches from interacting to noninteracting models, *J. Stat. Mech.* (2014) P07024.
 - ⁹⁷ E. Ilievski, J. De Nardis, B. Wouters, J.-S. Caux, F. H. L. Essler, and T. Prosen, Complete Generalized Gibbs Ensembles in an Interacting Theory, *Phys. Rev. Lett.* **115**, 157201 (2015).
 - ⁹⁸ V. Alba, Simulating the Generalized Gibbs Ensemble (GGE): a Hilbert space Monte Carlo approach, arXiv:1507.06994.
 - ⁹⁹ F. H. L. Essler, G. Mussardo, and M. Panfil, Generalized Gibbs ensembles for quantum field theories, *Phys. Rev. A* **91**, 051602 (2015).
 - ¹⁰⁰ J. Cardy, Quantum quenches to a critical point in one dimension: some further results, *J. Stat. Mech.* (2016) 023103.
 - ¹⁰¹ S. Sotiriadis, Memory-preserving equilibration after a quantum quench in a 1d critical model, *Phys. Rev. A* **94**, 031605 (2016).
 - ¹⁰² A. Bastianello and S. Sotiriadis, Quasi locality of the GGE in interacting-to-free quenches in relativistic field theories, arXiv:1608.00924.
 - ¹⁰³ E. Vernier and A. C. Cubero, Quasilocal charges and the complete GGE for field theories with non diagonal scattering, arXiv:1609.03220.
 - ¹⁰⁴ L. Vidmar and M. Rigol, Generalized Gibbs ensemble in integrable lattice models, *J. Stat. Mech.* 064007 (2016).
 - ¹⁰⁵ C. Gogolin and J. Eisert, Equilibration, thermalisation, and the emergence of statistical mechanics in closed quantum systems, *Rep. Prog. Phys.* **79**, 056001 (2016).
 - ¹⁰⁶ Essler FHL and Fagotti M. Quench dynamics and relaxation in isolated integrable quantum spin chains. *J. Stat. Mech.* (2016) 064002.
 - ¹⁰⁷ P. Calabrese, F. H. L. Essler, and G. Mussardo, Introduction to “Quantum Integrability in Out of Equilibrium Systems” (2016) 064001.
 - ¹⁰⁸ L. Piroli, B. Pozsgay, and E. Vernier, From the Quantum Transfer Matrix to the Quench Action: The Loschmidt echo in the XXZ Heisenberg spin chains, *J. Stat. Mech.* (2017) P023106.
 - ¹⁰⁹ L. Piroli, E. Vernier, P. Calabrese, and M. Rigol, Correlations and diagonal entropy after quantum quenches in XXZ chains, *Phys. Rev. B* **95**, 054308 (2017).
 - ¹¹⁰ L. Bonnes, F. H. L. Essler, A. M. Läuchli, “Light-cone” dynamics after quantum quenches in spin chains, *Phys. Rev. Lett.* **113**, 187203 (2014).
 - ¹¹¹ J.-S. Caux, and F. H. L. Essler, Time evolution of local observables after quenching to an integrable model, *Phys. Rev. Lett.* **110**, 257203 (2013).
 - ¹¹² B. Wouters, M. Brockmann, J. De Nardis, D. Fioretto, M. Rigol, and J.-S. Caux, Quenching the Anisotropic Heisenberg Chain: Exact Solution and Generalized Gibbs Ensemble Predictions, *Phys. Rev. Lett.* **113**, 117202 (2014).
 - ¹¹³ B. Pozsgay, M. Mestyán, M. A. Werner, M. Kormos, G. Zaránd, and G. Takács, Correlations after Quantum Quenches in the XXZ Spin Chain: Failure of the Generalized Gibbs Ensemble, *Phys. Rev. Lett.* **113**, 117203 (2014).
 - ¹¹⁴ B. Bertini, D. Schuricht, and F. H. L. Essler, Quantum quench in the sine-Gordon model, *J. Stat. Mech.* (2014) P10035.
 - ¹¹⁵ J. De Nardis, B. Wouters, M. Brockmann, and J.-S. Caux, Solution for an interaction quench in the Lieb-Liniger Bose gas, *Phys. Rev. A* **89**, 033601 (2014).
 - ¹¹⁶ L. Bucciantini, Stationary State After a Quench to the Lieb-Liniger from Rotating BECs, *J. Stat. Phys.* **164**, 621 (2016).
 - ¹¹⁷ V. Alba and P. Calabrese, The quench action approach in finite integrable spin chains, *J. Stat. Mech.* (2016), 043105.
 - ¹¹⁸ L. Piroli, P. Calabrese, and F. H. L. Essler, Multiparticle Bound-State Formation following a Quantum Quench to the One-Dimensional Bose Gas with Attractive Interactions, *Phys. Rev. Lett.* **116**, 070408 (2016).
 - ¹¹⁹ L. Piroli, P. Calabrese, and F. H. L. Essler, Quantum quenches to the attractive one-dimensional Bose gas: exact results, *SciPost Phys.* **1**(1), 001 (2016).
 - ¹²⁰ M. Mestyán, B. Pozsgay, G. Takács, and M. A. Werner MA. Quenching the XXZ spin chain: quench action approach versus generalized Gibbs ensemble, *J. Stat. Mech.* (2015) P04001.
 - ¹²¹ M. Brockmann, B. Wouters, D. Fioretto, J. De Nardis, R. Vlijm, and J.-S. Caux, Quench action approach for releasing the Neel state into the spin-1/2 XXZ chain, *J. Stat. Mech.* (2014) P12009.
 - ¹²² E. Ilievski, E. Quinn, J. De Nardis, and M. Brockmann, String-charge duality in integrable lattice models, *J. Stat. Mech.* (2016) 063101.
 - ¹²³ L. Piroli, E. Vernier, and P. Calabrese, Exact steady states for quantum quenches in integrable Heisenberg spin chains, *Phys. Rev. B* **94**, 054313 (2016).
 - ¹²⁴ B. Bertini, L. Piroli, and P. Calabrese, Quantum quenches in the sinh-Gordon model: steady state and one-point correlation functions, *J. Stat. Mech.* (2016) 063102.
 - ¹²⁵ J.-S. Caux, The Quench Action, *J. Stat. Mech.* (2016) 064006.
 - ¹²⁶ B. Doyon, Exact large-scale correlations in integrable systems out of equilibrium, arXiv:1711.04568.
 - ¹²⁷ M. Ljubotina, M. Znidaric, and T. Prosen, *Nat. Commun.* **8**, 16117 (2017).
 - ¹²⁸ G. Misguich, K. Mallick, and P. L. Krapivsky, arXiv:1708.01843.
 - ¹²⁹ J.-M. Stephan, *J. Stat. Mech.* 103108 (2017).
 - ¹³⁰ S. R. White and A. E. Feiguin, Real-Time Evolution Using the Density Matrix Renormalization Group, *Phys. Rev. Lett.* **93**, 076401 (2004).
 - ¹³¹ A. J. Daley, C. Kollath, U. Schollwöck, and G. Vidal, Time-dependent density-matrix renormalization-group using adaptive effective Hilbert spaces, *J. Stat. Mech.* (2004) P04005.
 - ¹³² U. Schollwöck, The density-matrix renormalization group, *Rev. Mod. Phys.* **77**, 259 (2005).
 - ¹³³ U. Schollwöck, The density-matrix renormalization group in the age of matrix product states, *Annals of Physics* **326**, 96 (2011).
 - ¹³⁴ Our tDMRG simulations are implemented using the ITENSOR library (<http://itensor.org/>).
 - ¹³⁵ E. Levitan, F. Pollmann, J. H. Bardarson, and E. Altman, Quantum thermalization dynamics with Matrix-Product States,

arXiv:1702.08894.

- ¹³⁶ V. Eisler, Z. Zimboras, Area law violation for the mutual information in a nonequilibrium steady state, *Phys. Rev. A* **89**, 032321 (2014).
- ¹³⁷ M. Kormos, Z. Zimborás, Temperature driven quenches in the Ising model: appearance of negative Rényi mutual information, *J. Phys. A: Math. Theor.* **50** 264005 (2017).
- ¹³⁸ E. Mascarenhas, G. Giudice, and V. Savona, arxiv:1703.02934.
- ¹³⁹ L. Piroli, J. De Nardis, M. Collura, B. Bertini, and M. Fagotti, Transport in out-of-equilibrium XXZ chains: non-ballistic behavior and correlation functions, *Phys. Rev. B* **96**, 115124 (2017).
- ¹⁴⁰ P. Ruggiero, V. Alba, and P. Calabrese, Entanglement negativity in random spin chains, *Phys. Rev. B* **94**, 035152 (2016).